Dossier

This paper is a part of the hereunder thematic dossier published in OGST Journal, Vol. 69, No. 4, pp. 507-766 and available online here

Cet article fait partie du dossier thématique ci-dessous publié dans la revue OGST, Vol. 69, n°4 pp. 507-766 et téléchargeable ici

DOSSIER Edited by/Sous la direction de : **Z. Benjelloun-Touimi**

Geosciences Numerical Methods
Modélisation numérique en géosciences

ifp Energies nouvelles

D o s s i e r

Geosciences Numerical Methods
Modélisation numérique en géosciences

An Efficient XFEM Approximation of Darcy Flows in Arbitrarily Fractured Porous Media

Alessio Fumagalli* and Anna Scotti

MOX – Modellistica e Calcolo Scientifico, Dipartimento di Matematica "F. Brioschi", Politecnico di Milano, via Bonardi 9, 20133 Milan - Italy
e-mail: alessio.fumagalli@mail.polimi.it - anna.scotti@mail.polimi.it

* Corresponding author

Résumé — **Une approximation efficace par XFEM pour écoulements de Darcy dans les milieux poreux arbitrairement fracturés** — Les écoulements souterrains sont fortement influencés par la présence de failles et de grandes fractures qui modifient la perméabilité du milieu agissant comme des barrières ou des conduits pour l'écoulement. Une description précise des propriétés hydrauliques des fractures est donc essentielle pour la modélisation de la migration du pétrole ou de l'exploitation de ressources non conventionnelles. Toutefois, la largeur de fractures est souvent petite par rapport à la taille typique des éléments du maillage. Pour résoudre le problème par une approximation numérique obtenue sans raffinement du maillage, on remplace les fractures par des surfaces immergées dans la matrice poreuse. Par ailleurs, on veut permettre aux surfaces d'être indépendantes par rapport à la structure du maillage, en manipulant les discontinuités à l'intérieur des éléments par la méthode des éléments finis étendus (XFEM *Extended Finite Element Method*). On utilise une technique similaire pour obtenir un outil plus flexible, apte à la résolution du problème dans les régions d'intersection potentielles entre les fractures.

Abstract — *An Efficient XFEM Approximation of Darcy Flows in Arbitrarily Fractured Porous Media* — *Subsurface flows are influenced by the presence of faults and large fractures which act as preferential paths or barriers for the flow. In literature models were proposed to handle fractures in a porous medium as objects of codimension 1. In this work we consider the case of a network of intersecting fractures, with the aim of deriving physically consistent and effective interface conditions to impose at the intersection between fractures. This new model accounts for the angle between fractures at the intersections and allows for jumps of pressure across the intersection. This latter property permits to describe more accurately the flow when fractures are characterised by different properties, than other models that impose pressure continuity. The main mathematical properties of the model, derived in the two-dimensional setting, are analysed. As concerns the numerical discretization we allow the grids of the fractures to be independent, thus in general non-matching at the intersection, by means of the Extended Finite Element Method (XFEM), to increase the flexibility of the method in the case of complex geometries characterised by a high number of fractures.*

INTRODUCTION

Subsurface flows are strongly influenced by the presence of fractures. While small and micro-fractures can be easily accounted for by means of upscaling techniques, large fractures and faults play a more complex role, acting as paths or barriers for the flow. These effects are very relevant for many applications such as oil migration, oil recovery, CO_2 storage and groundwater contamination and remediation.

Due to the spatial scales involved, the simulation of fractured porous media is a very challenging task. The typical size of these features, compared to the domain size, is usually such that a very fine mesh is needed to resolve the fracture width. Moreover, in realistic cases, the porous media are usually crossed by a large number of fractures that can intersect each other. If we consider the finite element method on an unstructured tetrahedral grid the construction of a good computational grid is essential to achieve accurate results. However, the conformity of the grid to possibly numerous and intersecting fractures can be a strong constraint and can affect the quality of the elements. Besides, the mesh refinement required to capture the faults or fractures aperture leads to a very high, if not unaffordable, computational cost.

These problems can be in part overcome with the model reduction strategy proposed in [1, 2] and later extended in [3]. It consists in a domain decomposition approach where the fractures are regarded as $n-1$ dimensional interfaces inside a n-dimensional porous matrix, *i.e.* surfaces in 3D or lines in 2D. This approach can effectively reduce the number of unknowns in simulations because it removes the need for fine grids inside the fractures [4, 5]. However, the aforementioned works are restricted to the case of grids that follow the shape of faults and fractures. In [6], the authors remove the constraint of mesh conformity by means of the Extended Finite Element Method (XFEM) [7], allowing the fracture to cross the elements of the grid in an arbitrary way. The XFEM are widely used in the simulation of the mechanics of fractured media, while their application to flow problems in the presence of fractures and heterogeneities is still at the beginning. This approach has reduced the effort in constructing the computational grid, since this operation does not have to account for the possibly complicated geometry of the fractures and, moreover, can be performed only once even if the position of fractures or faults changes due to multiple scenarios or sensitivity analysis. The method was, however, limited to the case of one interface, or at most, of more non intersecting interfaces [4]. The difficulty in dealing with intersecting fractures is twofold. On one hand, suitable coupling conditions have to be introduced at the intersections between two or more fractures. Furthermore, in an XFEM approach, the elements of the mesh that are crossed by more than one interface require an additional enrichment of the finite element space. Realistic simulations of intersecting faults in a three dimensional domain are presented in [8], where the continuity of pressure and mass conservation are enforced at the intersections. More general coupling conditions are introduced and discussed in [9] to account for different properties of the fractures allowing for pressure and velocity jumps at the intersection, similarly to the conditions derived in [2] for the matrix-fracture system. The aforementioned work [9] considers the case of a network isolated by the porous matrix, in the limit case where the matrix can be regarded as impermeable with respect to the fractures. The case of an isolated fracture network in an impermeable matrix is also tackled in [9] by means of the XFEM method and an optimization strategy to enforce the coupling conditions at the intersections. In this paper, we present a discretization strategy for the fully coupled problem of porous media crossed by intersecting fractures, where the fractures exchange fluid between each other, and with the porous matrix surrounding them. To obtain a method that is as flexible as possible, in the view of future realistic applications, we employ the XFEM on two levels. First of all, we allow the grid of the medium to be non-conforming with the fractures. Moreover, we allow the grids of the fractures to be arbitrary, *i.e.* non-matching at the intersection, and handle the pressure and velocity jumps at the intersection points with $n-1$ dimensional extended finite elements, as done in [9]. A particular attention is devoted to the enrichment of the finite element spaces in the elements crossed by two fractures, where we extend the method proposed by [10] to allow the solution to be discontinuous across the two interfaces. In this work, we have restricted ourselves to the case where each triangle is crossed at most by two fractures, and each intersection involves at most two fractures. The first hypothesis could be removed with a further enrichment of the finite element space in the cut elements, and a resulting increase in code complexity and computational cost. The second hypothesis instead is related to the coupling conditions derived in [9] that are limited to the case of at most two fractures intersecting in a point. Removing this assumption will thus require the derivation of more general coupling conditions and will be the subject of future works. Finally, we point out that a large variety of method is available in literature for the simulation of underground flows in presence of fractures, using discrete fracture models with conforming meshes [11, 12].

The paper is structured as follows: in Section 1, we present both the physical equations and the reduced

model, with the interface conditions that couple the matrix-fracture system and the fracture-fracture system. In Section 2, we present the numerical discretization of the problem with an highlight on the enrichment of the finite element spaces. In Section 3, we present some numerical experiments to asses the effectiveness of the proposed method. Finally, the last section is devoted to conclusions and to ongoing works.

1 MATHEMATICAL MODEL

We call fracture, or fault, a region of the porous medium with data that differ of several order of magnitude from the neighbouring medium. While the thickness of these regions is very small the extension is comparable with the domain size. In the following analyses, we consider only the case of two intersecting fractures with only one intersection region. Nevertheless, the results presented can be extended, rather easily and under the forthcoming hypotheses, to the case of several fractures with several intersections. Examples can be found in Section 3.

1.1 Physical Equations

Let us consider a domain $D \subset \mathbb{R}^2$, crossed by two intersecting fractures called $\Omega_1, \Omega_2 \subset D$. Here and in the sequel, we indicate with the lower case subscript i the restriction of data and unknowns to Ω_i. We assume that the intersection region, called $\mathcal{I} := \Omega_1 \cap \Omega_2$, forms a connected subset of each Ω_i, *i.e.* we allow only one intersection between the fractures. For simplicity, we assume that $\mathcal{I}$ can be approximated by a quadrilateral with parallel sides. Given $\mathcal{I}$, each fracture Ω_i can be written as the union of disjoint sets $\Omega_i = \Omega_{i1} \cup \mathcal{I} \cup \Omega_{i2}$, the two non-empty branches Ω_{ij} of the fracture and the intersecting region. We indicate with the lower case subscript ij and the subscripts $\mathcal{I}$ the restriction of data and unknowns to Ω_{ij} and to $\mathcal{I}$, respectively. Finally, thanks to the

previous splitting of D, we define the surrounding porous medium to the fractures as $\Omega := D\backslash(\Omega_1 \cup \Omega_2)$. Figure 1 shows an example of the domain subdivision.

We divide the boundary of each fracture Ω_i into three disjoint pieces $\gamma_{i,1}$, $\gamma_{i,2}$ and a part common with ∂D, as Figure 1 shows. More precisely, we indicate as $\gamma_{i,2}$ the boundary of Ω_i contained in Ω in the direction of $\boldsymbol{n}_i$, $\boldsymbol{n}_i$ being the inward, with respect to Ω_i, unit normal to $\gamma_{i,1}$, *vice versa* for $\gamma_{i,1}$.

Following [2, 9], we introduce the thickness d_i of Ω_i, which is a regular function of the center line γ_i of Ω_i. We can write each fracture Ω_i as:

$$\Omega_i = \left\{ \boldsymbol{x} \in \mathbb{R}^2 \,:\, \boldsymbol{x} = \boldsymbol{s} + r\boldsymbol{n}_i,\, \boldsymbol{s} \in \gamma_i, r \in \left(-\frac{d_i(\boldsymbol{s})}{2}, \frac{d_i(\boldsymbol{s})}{2} \right) \right\}$$

We are interested in computing the steady pressure field p and the velocity field $\boldsymbol{u}$ in the whole domain D, which are governed by the Darcy problem formulated in Ω, Ω_1, Ω_2 and $\mathcal{I}$ as:

$$\begin{cases} \begin{cases} \boldsymbol{K}^{-1}\boldsymbol{u} + \nabla p = \boldsymbol{0} \\ \nabla \cdot \boldsymbol{u} = f \end{cases} & \text{in } \Omega \\ \begin{cases} \boldsymbol{K}_j^{-1}\boldsymbol{u}_j + \nabla p_j = \boldsymbol{0} \\ \nabla \cdot \boldsymbol{u}_j = f_j \end{cases} & \text{in } \Omega_j \end{cases} \quad (1a)$$

for $j = \mathcal{I}, 1, 2$. Here, $\boldsymbol{K}$ and $\boldsymbol{K}_j$ denote the symmetric and positive definite permeability tensors and f and f_j the source terms. To couple all the problems in (1a), we use the classical interface conditions:

$$\begin{cases} \begin{cases} p_i = p \\ \boldsymbol{u}_i \cdot \boldsymbol{n}_i = \boldsymbol{u} \cdot \boldsymbol{n}_i \end{cases} & \text{on } \partial\gamma_{i,j} \\ \begin{cases} p_i = p_{\mathcal{I}} \\ \boldsymbol{u}_i \cdot \boldsymbol{n}_{\mathcal{I}} = \boldsymbol{u}_{\mathcal{I}} \cdot \boldsymbol{n}_{\mathcal{I}} \end{cases} & \text{on } \partial\mathcal{I} \end{cases} \quad (1b)$$

a)

b)
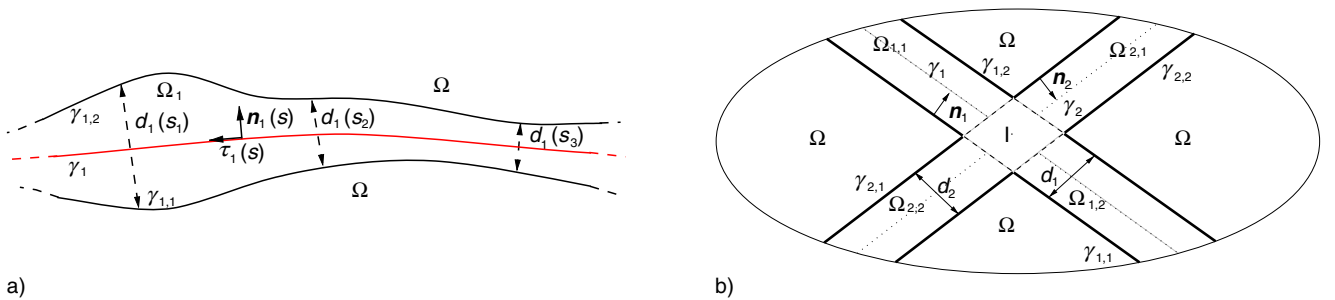
Figure 1

a) Example of a single fracture; we have $\boldsymbol{s}_k \in \gamma_1$; b) example of the set subdivision for a given problem.

for $i, j = 1, 2$. In (1b), we have indicated with $\boldsymbol{n}_\mathcal{I}$ the outward unit normal to $\mathcal{I}$. Finally we impose, for the sake of simplicity, homogeneous boundary condition on the pressure:

$$\begin{cases} p = 0 & \text{on } \partial D \cap \partial \Omega \\ p_i = 0 & \text{on } \partial D \cap \partial \Omega_i \end{cases} \quad (1c)$$

Following [13], it can be proven that problem (1) is well posed.

1.2 Reduced Model

In [2], a reduced model is derived for a single fracture coupled with the porous media, while in [9] a similar model is derived for networks of fractures uncoupled with the surrounding porous medium. We present a reduced model, based on the aforementioned works, which describes the coupling between a network of fractures and the porous medium obtaining a complete model for a single phase flow in fractured porous media.

We recall, for readers convenience, the main idea for both models. We start by collapsing each Ω_i with its centre line γ_i, with normal $\boldsymbol{n}_i$, and consider the following domain $\Omega \bigcup_i \gamma_i$ for the problem. Given a regular function $a : \Omega \to \mathbb{R}^m$, with $m = 1$ or 2, defined on both side of the generic fracture γ, let us define:

$$a_i(\boldsymbol{x}) := \lim_{\varepsilon \to 0^+} a\big(\boldsymbol{x} + (-1)^i \varepsilon \boldsymbol{n}(\boldsymbol{x})\big) \quad \text{for } i = 1, 2 \quad (2)$$

with $\boldsymbol{x} \in \gamma$ and $\boldsymbol{n}(\boldsymbol{x})$ the normal of γ at $\boldsymbol{x}$. Given (2), the jump and mean operators across γ are $[\![a]\!]_\gamma := a_1 - a_2$ and $\{a\}_\gamma := (a_1 + a_2)/2$, respectively. We define the intersection point between the two fractures γ_1 and γ_2 as $\boldsymbol{i}_p := \gamma_1 \cap \gamma_2$. Given a function $b : \gamma_i \to \mathbb{R}^m$, with $m = 1$ or 2, defined on both sides of the generic intersection point $\boldsymbol{i}_p$, let us define:

$$a_{ij} := \lim_{\varepsilon \to 0^+} a_i\big(\boldsymbol{i}_p + (-1)^j \varepsilon \boldsymbol{\tau}_{i,\boldsymbol{i}_p}\big) \quad \text{for } j = 1, 2 \quad (3)$$

where $\boldsymbol{\tau}_{i,\boldsymbol{i}_p}$ denotes the tangential unit vector $\boldsymbol{\tau}_i$ at the intersection point $\boldsymbol{i}_p$, see [9]. As we done previously, given (3), we introduce the jump and mean operators across the intersection point $\boldsymbol{i}_p$, for $i = 1, 2$, as $[\![a]\!]_{\boldsymbol{i}_p} := a_{i1} - a_{i2}$ and $\{a_i\}_{\boldsymbol{i}_p} := (a_{i1} + a_{i2})/2$. We define the projection matrix on the normal space as $\boldsymbol{N}_i := \boldsymbol{n}_i \otimes \boldsymbol{n}_i$ and on the tangential space as $\boldsymbol{T}_i := \boldsymbol{I} - \boldsymbol{N}_i$. Given a regular function $a : \Omega_i \to \mathbb{R}$ the tangential operators are $\nabla_{\boldsymbol{\tau}_i} a := \boldsymbol{T}_i \nabla a$ and $\nabla_{\boldsymbol{\tau}_i} \cdot a := \boldsymbol{T}_i : \nabla a$. Following [2, 9], we suppose that $\boldsymbol{K}_i = K_{i,\boldsymbol{n}} \boldsymbol{N}_i + K_{i,\boldsymbol{\tau}} \boldsymbol{T}_i$ in $\Omega_i \backslash \mathcal{I}$ with $K_{i,\cdot}$ positive, while $\boldsymbol{K}_\mathcal{I}$

is constant in $\mathcal{I}$. We will indicate with $\hat{\cdot}$ the reduced variables defined in each γ_i. We introduce, for each fracture γ_i, the reduced velocity $\hat{\boldsymbol{u}}_i$ as:

$$\hat{\boldsymbol{u}}_i(\boldsymbol{s}_i) := \int_{-\frac{d_i}{2}}^{\frac{d_i}{2}} \boldsymbol{T}_i \boldsymbol{u}_i(\boldsymbol{s}_i + r\boldsymbol{n}_i) dr$$

and pressure $\hat{p}_i$ as:

$$\hat{p}_i(\boldsymbol{s}_i) := \frac{1}{d_i} \int_{-\frac{d_i}{2}}^{\frac{d_i}{2}} p_i(\boldsymbol{s}_i + r\boldsymbol{n}_i) dr,$$

with $\boldsymbol{s}_i \in \gamma_i$. Moreover, the reduced source term $\hat{f}_i$ and the inverse of the scaled permeabilities η_{γ_i} and $\hat{\eta}_i$ are defined as:

$$\hat{f}_i(\boldsymbol{s}_i) := \int_{-\frac{d_i}{2}}^{\frac{d_i}{2}} f_i(\boldsymbol{s}_i + r\boldsymbol{n}_i) dr$$

$$\eta_{\gamma_i} := \frac{d_i}{K_{i,\boldsymbol{n}}} \quad \text{and} \quad \hat{\eta}_i := \frac{1}{d_i K_{i,\boldsymbol{\tau}}}$$

We define $d_i^* := d_i / \sin \theta$, with θ the angle between the two fractures at $\boldsymbol{i}_p$. The reduction process approximates the pressure in the intersection region $\mathcal{I}$ to a scalar value $\hat{p}_\mathcal{I}$ in $\boldsymbol{i}_p$:

$$\hat{p}_\mathcal{I} := \frac{1}{|\mathcal{I}|} \int_\mathcal{I} p_\mathcal{I}(\boldsymbol{x}) d\boldsymbol{x}$$

The reduced source term $f_\mathcal{I}$ is defined as:

$$\hat{f}_\mathcal{I} := \int_\mathcal{I} f_\mathcal{I}(\boldsymbol{x}) d\boldsymbol{x}$$

Moreover we indicate the inverse of the reduced permeability, along the directions $\boldsymbol{\tau}_{i,\boldsymbol{i}_p}$ and $\boldsymbol{\tau}_{j,\boldsymbol{i}_p}$, in the intersection as $\eta_{ij}^\mathcal{I} := \boldsymbol{\tau}_{i,\boldsymbol{i}_p}^\mathrm{T} \cdot \boldsymbol{K}_\mathcal{I}^{-1} \boldsymbol{\tau}_{j,\boldsymbol{i}_p}$.

The complete reduced model that describes the evolution of $\boldsymbol{u}, p, \hat{\boldsymbol{u}}_i, \hat{p}_i$ and $\hat{p}_\mathcal{I}$ consists of the following system of partial differential equations, for $i = 1, 2$:

$$\begin{cases} \boldsymbol{K}^{-1} \boldsymbol{u} + \nabla p = \boldsymbol{0} & \\ \nabla \cdot \boldsymbol{u} = f & \text{in } \Omega \\ p = 0 & \text{on } \partial D \cap \partial \Omega \\ \hat{\eta}_i \hat{\boldsymbol{u}}_i + \nabla_{\boldsymbol{\tau}_i} \hat{p}_i = \boldsymbol{0} & \\ \nabla_{\boldsymbol{\tau}_i} \cdot \hat{\boldsymbol{u}}_i = \hat{f}_i + [\![\boldsymbol{u} \cdot \boldsymbol{n}_i]\!]_{\gamma_i} & \text{in } \gamma_i \backslash \boldsymbol{i}_p \\ \hat{p}_i = 0 & \text{on } \partial \gamma_i \end{cases} \quad (4a)$$
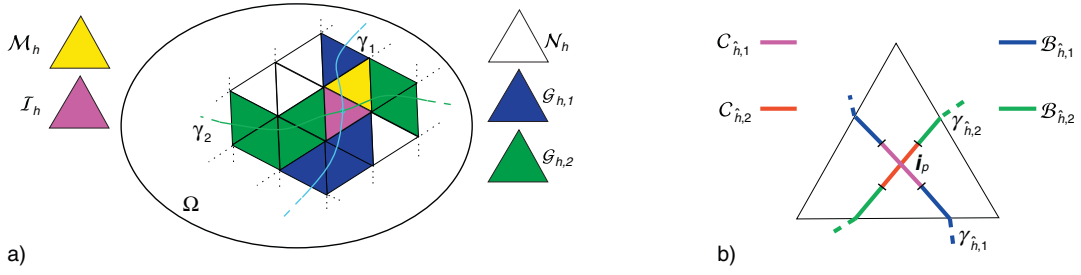
Figure 2

a) Example of the subdivision of $\mathcal{T}_h$ into uncut elements, elements crossed by one fracture and elements crossed by two fractures with and without an intersection; b) subdivision of $\gamma_{\hat{h},i}$.

coupled with the interface conditions for the matrix-fracture system for $j = 1, 2$:

$$\begin{cases} \xi_{0i}\eta_{\gamma i}[\![\boldsymbol{u} \cdot \boldsymbol{n}_i]\!]_{\gamma_i} = \{p\}_{\gamma i} - \hat{p}_i \\ \eta_{\gamma i}\{\boldsymbol{u} \cdot \boldsymbol{n}_i\}_{\gamma i} = [\![p]\!]_{\gamma i} \end{cases} \quad \text{on } \gamma_i \quad (4b)$$

with $\xi_{0j} \in [0, 0.25]$ a first model closure parameter, see [2, 3] for its meaning. Moreover, the coupling conditions for the fracture-fracture system for $i \neq j = 1, 2$ are:

$$\begin{cases} \displaystyle\sum_{k=1}^{2} [\![\hat{\boldsymbol{u}}_k \cdot \boldsymbol{\tau}_k]\!]_{\boldsymbol{i}_p} = \hat{f}_{\mathcal{I}} \\ \displaystyle\frac{|I|}{d_i} \sum_{k=1}^{2} \frac{\eta_{ik}^{\mathcal{I}}}{d_k^*} \{\hat{\boldsymbol{u}}_k \cdot \boldsymbol{\tau}_k\}_{\boldsymbol{i}_p} = [\![\hat{p}_i]\!]_{\boldsymbol{i}_p} \quad \text{in } \boldsymbol{i}_p \\ \hat{\xi}_0 \frac{d_j}{d_i} \eta_{ii}^{\mathcal{I}} [\![\hat{\boldsymbol{u}}_k \cdot \boldsymbol{\tau}_i]\!]_{\boldsymbol{i}_p} = \{\hat{p}_i\}_{\boldsymbol{i}_p} - \hat{p}_{\mathcal{I}} \end{cases} \quad (4c)$$

Bounds for the value of the second closure parameter $\hat{\xi}_0$ are discussed in [9].

2 NUMERICAL DISCRETIZATION

The discretization of (4) is based on the XFEM method [7] for both the porous medium and the intersecting fractures. In fact, we allow non-matching grids between the fractures and the porous media and in the intersection point of the intersecting fractures. To this purpose, we introduce suitable enriched finite element spaces based on the standard Raviart-Thomas finite element $\mathbb{RT}_0$, for vector fields, and piecewise constant finite element $\mathbb{P}_0$, for scalar fields.

We consider a family of regular tessellations $\mathcal{T}_h$, $h := \max_{K \in \mathcal{T}_h} \text{diam}(K)$, with $\partial\mathcal{T}_h := \{e \in \partial K, K \in \mathcal{T}_h\}$. For each fracture i, we introduce a family of regular tessellations $\gamma_{\hat{h},i}$ with $\hat{h} := \max_{l \in \gamma_{\hat{h},i}} |l|$. We suppose that if a

fracture intersects a triangle then it intersects exactly two edges, [10]. Moreover, for the sake of simplicity, we suppose that at most two fractures cross a triangle and, if an intersection occurs, it happens inside a triangle. There last two assumptions could be removed with a generalization of the FEM space and the implementation. We introduce the following subsets of $\mathcal{T}_h$, for $i \neq j$ and for $i, j = 1, 2$:

$$\mathcal{I}_h := \{K \in \mathcal{T}_h : (\gamma_i \cap \gamma_j \neq \emptyset) \in K\}$$
$$\mathcal{M}_h := \{K \in \mathcal{T}_h : K \cap \gamma_i \neq \emptyset \wedge K \cap \gamma_j \neq \emptyset\} \setminus \mathcal{I}_h$$
$$\mathcal{G}_{h,i} := \{K \in \mathcal{T}_h : K \cap \gamma_i \neq \emptyset \wedge K \cap \gamma_j = \emptyset\}$$
$$\mathcal{CR}_h := \mathcal{M}_h \cup \mathcal{I}_h \cup \mathcal{G}_{h,1} \cup \mathcal{G}_{h,2} \text{ and}$$
$$\mathcal{N}_h := \mathcal{T}_h \setminus \mathcal{CR}_h$$

As shown in Figure 2, $\mathcal{I}_h$ denotes the element that contains the intersection between the fractures, $\mathcal{M}_h$ contains the elements that are crossed by both fractures but do not contain the intersection point, while $\mathcal{G}_{h,i}$ contains the elements crossed only by the i-th fracture. The last two subsets are the cut region and the collection of elements in $\mathcal{T}_h$ not crossed by any fracture, respectively. We split also the mesh of the fractures into intersected elements and non intersected elements, in particular, we define for $i = 1, 2$:

$$\mathcal{C}_{\hat{h},i} := \{l \in \gamma_{\hat{h},i} : l \cap \boldsymbol{i}_p \neq \emptyset\} \quad \text{and} \quad \mathcal{B}_{\hat{h},i} := \gamma_{\hat{h},i} \setminus \mathcal{C}_{\hat{h},i}$$

Figure 2 for an example. With this subdivision, we define the following enriched finite elements spaces for the medium:

$$\widetilde{\mathbb{RT}}_0(\mathcal{T}_h) := \mathbb{RT}_0(\mathcal{N}_h) \oplus \bigoplus_{k,j=1}^{2} \mathbb{RT}_0(\mathcal{G}_{h,k})$$

$$\oplus \bigoplus_{m=1}^{3} \mathbb{RT}_0(\mathcal{M}_h) \oplus \bigoplus_{l=1}^{4} \mathbb{RT}_0(\mathcal{I}_h)$$
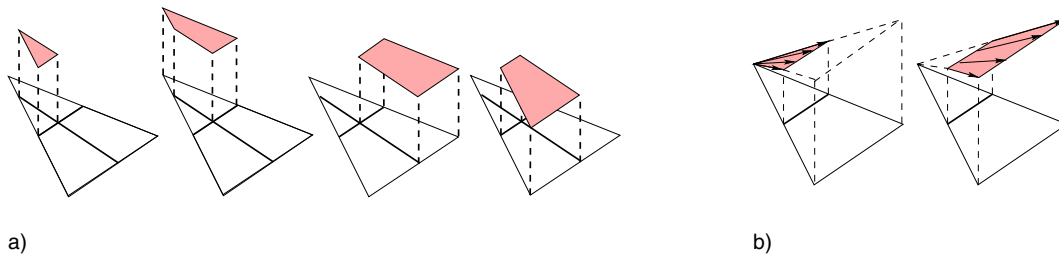
Figure 3

Examples of some base functions for cut elements. a) Example of $\mathbb{P}_0(\mathcal{I}_h)$; b) example of $\mathbb{RT}_0(\mathcal{G}_h)$.

furthermore, we have:

$$\widetilde{\mathbb{P}}_0(\mathcal{T}_h) := \mathbb{P}_0(\mathcal{N}_h) \oplus \bigcup_{k,j=1}^{2} \mathbb{P}_0(\mathcal{G}_{h,k})$$

$$\oplus \bigcup_{m=1}^{3} \mathbb{P}_0(\mathcal{M}_h) \oplus \bigcup_{l=1}^{4} \mathbb{P}_0(\mathcal{I}_h)$$

With these definitions, we can represent, for both p and $\boldsymbol{u}$, four discontinuities in the elements in $\mathcal{I}_h$, two in $\mathcal{M}_h$ and one in $\mathcal{G}_{h,k}$. An example is reported in Figure 3.

Moreover for each fracture $i = 1, 2$, the enriched finite elements spaces are:

$$\widetilde{\mathbb{RT}}_0\left(\gamma_{\hat{h},i}\right) := \mathbb{RT}_0\left(\mathcal{B}_{\hat{h},i}\right) \oplus \bigcup_{k=1}^{2} \mathbb{RT}_0\left(\mathcal{C}_{\hat{h},i}\right)$$

$$\widetilde{\mathbb{P}}_0\left(\gamma_{\hat{h},i}\right) := \mathbb{P}_0\left(\mathcal{B}_{\hat{h},i}\right) \oplus \bigcup_{k=1}^{2} \mathbb{P}_0\left(\mathcal{C}_{\hat{h},i}\right)$$

Using a standard procedure, we can write problem (4) in its discrete counterpart, see [6, 9] for more details. Hence the global algebraic system is a symmetric block-saddle problem $\boldsymbol{Gx} = \boldsymbol{b}$, with:

$$\boldsymbol{G} = \begin{bmatrix} \boldsymbol{A} & \boldsymbol{B} & \boldsymbol{0} & \boldsymbol{E}_1 & \boldsymbol{0} & \boldsymbol{E}_2 & \boldsymbol{0} \\ \boldsymbol{B}^{\mathrm{T}} & \boldsymbol{0} & \boldsymbol{0} & \boldsymbol{0} & \boldsymbol{0} & \boldsymbol{0} & \boldsymbol{0} \\ \boldsymbol{0} & \boldsymbol{0} & \hat{\boldsymbol{A}}_1 & \hat{\boldsymbol{B}}_1 & \boldsymbol{0} & \boldsymbol{0} & \hat{\boldsymbol{E}}_1 \\ \boldsymbol{E}_1^{\mathrm{T}} & \boldsymbol{0} & \hat{\boldsymbol{B}}_1^{\mathrm{T}} & \boldsymbol{0} & \boldsymbol{0} & \boldsymbol{0} & \boldsymbol{0} \\ \boldsymbol{0} & \boldsymbol{0} & \boldsymbol{0} & \boldsymbol{0} & \hat{\boldsymbol{A}}_2 & \hat{\boldsymbol{B}}_2 & \hat{\boldsymbol{E}}_2 \\ \boldsymbol{E}_2^{\mathrm{T}} & \boldsymbol{0} & \boldsymbol{0} & \boldsymbol{0} & \hat{\boldsymbol{B}}_2^{\mathrm{T}} & \boldsymbol{0} & \boldsymbol{0} \\ \boldsymbol{0} & \boldsymbol{0} & \hat{\boldsymbol{E}}_2^{\mathrm{T}} & \boldsymbol{0} & \hat{\boldsymbol{E}}_2^{\mathrm{T}} & \boldsymbol{0} & \boldsymbol{0} \end{bmatrix}$$

$$\boldsymbol{x} = [\boldsymbol{u}, p, \hat{\boldsymbol{u}}_1, \hat{p}_1, \hat{\boldsymbol{u}}_2, \hat{p}_2, \hat{p}_{\mathcal{I}}]^{\mathrm{T}} \text{ and}$$

$$\boldsymbol{b} = \left[\boldsymbol{0}, \boldsymbol{F}_q, \boldsymbol{0}, \hat{\boldsymbol{F}}_1, \boldsymbol{0}, \hat{\boldsymbol{F}}_2, \hat{\boldsymbol{F}}_{\mathcal{I}}\right]^{\mathrm{T}}$$

The matrices $\boldsymbol{E}_i$ and $\hat{\boldsymbol{E}}_i$ account for the coupling between the matrix and the fractures and between the fractures at the intersection.

3 APPLICATIVE EXAMPLES

We present some examples and test cases to asses the reduced model presented in Section 1.2. Example 3.1 highlights the model error introduced using the reduced model instead of the physical equations, while Example 3.2 shows a synthetic test case.

3.1 Model Error

The model error is the error we commit if we use the reduced model (4) instead of solving the real equations (1).

We define the error $err(K)$, for each cell of the mesh, as the difference between a reference solution, obtained using the original equations solved on a fine grid, and the reduced solution. Moreover, we introduce the relative error normalized with the norm of the reference solution. The finer grid is a hierarchical refinement of the mesh $\mathcal{T}_h$. Both errors are:

$$err(K) := \|p - p_{ref}\|_{L^2(K)}$$
$$err_{rel}(K) := \frac{err(K)}{\|p_{ref}\|_{L^2(K)}} \qquad \forall K \in \mathcal{T}_h \qquad (5)$$

In the definition of the errors, we do not take into account the fractures but only their effect on the surrounding domain.

We consider a two-dimensional problem in a square domain $D = (0, 1)^2$ cut by two intersecting fractures characterized by different properties:

$$\gamma_1 = \{(x,y) \in \Omega : y = 0.387\} \text{ and}$$
$$\gamma_2 = \{(x,y) \in \Omega : y = -2x + 1.4\}$$
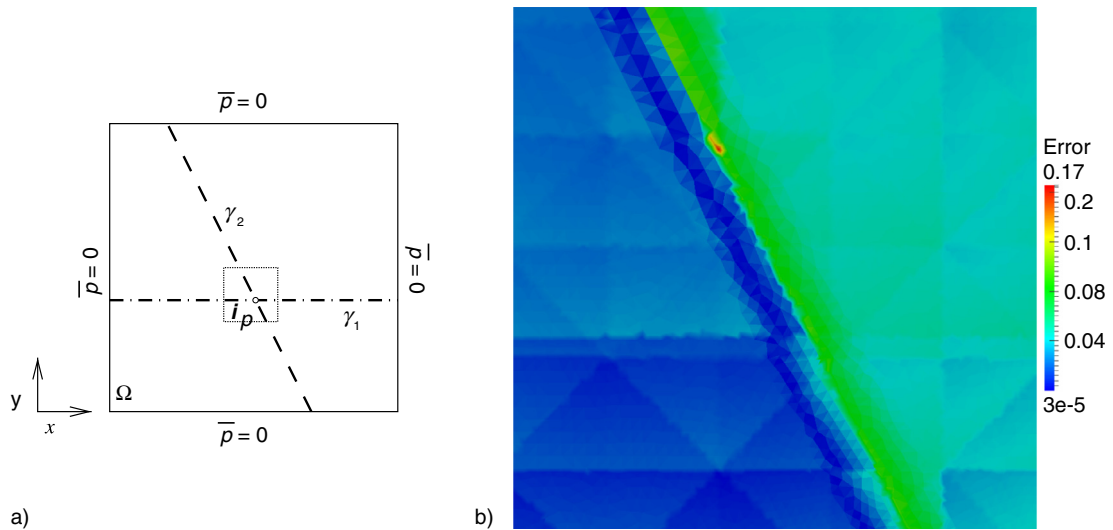
Figure 4

a) The computational domain and the zoom, coloured in green, of the domain Ω while b) the model error in the zoom for thickness $d = 0.02$, with shape parameter $\xi_0 = 0.25$.

On the boundaries of the domain $\partial\Omega$ and of each fracture $\partial\gamma_i$, for $i = 1, 2$, we prescribe homogeneous natural boundary conditions. The bulk flow and the flow in the intersecting fractures are described by (4) with source terms $f = 10$ and $\hat{f}_i = 10d$ with d the thickness of the fracture for both fractures, and $\boldsymbol{K} = \boldsymbol{I}$. Fracture γ_1 is characterized by the same tangential and normal permeability as the porous medium in Ω thus $\hat{\eta}_1 = d^{-1}$ and $\eta_{\gamma_1} = d$. Fracture γ_2 is instead characterized by the same tangential permeability as the porous medium in Ω, i.e. $\hat{\eta}_2 = d^{-1}$, and a low normal permeability such that $\eta_{\gamma_2} = 50d$. We set $\hat{\xi}_0 = 0$. The computational domain is sketched in Figure 4.

Figure 5 shows the pressure field in the domain Ω and in the fractures γ_1 and γ_2, obtained with and without the reduced model. Due to the small normal permeability of γ_2, there is a jump in the pressure across this fracture, while the effect of fracture γ_1 is null since it has the same permeability tensor as the porous matrix.

The global relative error (5) is reported in Table 1.

We notice that decreasing the thickness d of the fracture the model error decreases, while changing the shape parameter ξ_0 the model error does not change significantly. Figure 6 shows the model error (5) considering the global domain and the domain without the first fracture. We take as a reference the solution of the real problem with a fine grid composed by 114 115 triangles. Due to the model reduction the major errors are localized near the fractures, in particular when a pressure jump occurs across a fracture.

In Figure 4, we present a zoom of the error near the intersection point $\boldsymbol{i}_p$, we can notice that the error there is comparable with the neighbouring regions.

3.2 A synthetic Test Case

Let us consider a synthetic test case that aims at reproducing the quarter of five spots problem in the presence of fractures. The computational domain is the unit square and no flux boundary conditions are imposed on the edges. The presence of the injector well at the left bottom corner and the extracting well at the top right corner is mimicked with two source terms of equal intensity and opposite sign, i.e.:

$$f = \begin{cases} 1 & \text{if } x^2 + y^2 < 0.08 \\ -1 & \text{if } (1-x)^2 + (1-y)^2 < 0.08 \\ 0 & \text{otherwise} \end{cases}$$

The geometry of the fracture replicates one of the test cases proposed in [12] and there solved with the finite volume method on a grid conforming to the fractures. In particular, we have three fractures:

$$\gamma_1 = \{(x,y) \in \Omega : y = 0.2 \text{ and } 0 \leq x \leq 0.6\}$$
$$\gamma_2 = \{(x,y) \in \Omega : x = 0.3 \text{ and } 0 \leq y \leq 0.4\}$$
$$\gamma_3 = \{(x,y) \in \Omega : x = 0.7 \text{ and } 0.3 \leq x \leq 0.7\}$$
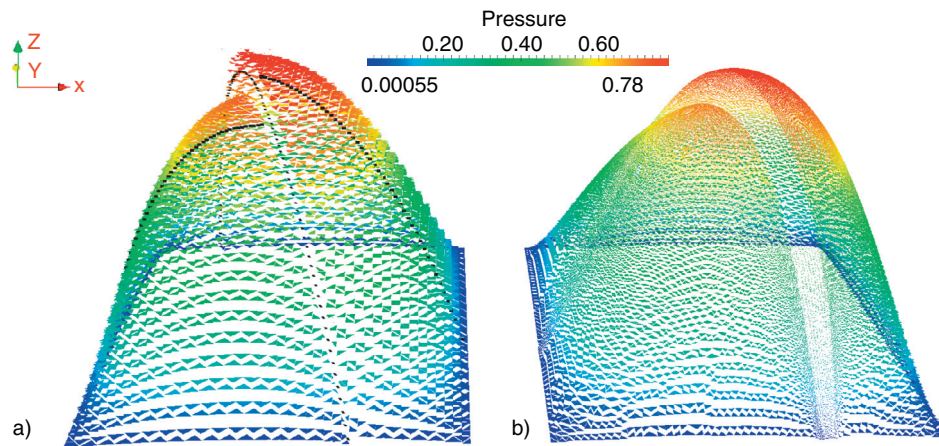
Figure 5

a) The solution with the reduced model, with $\xi_0 = 0.25$ and $d = 0.02$, using 4 418 triangles for the medium, 101 segments for first fracture and 102 segments for the second fractures, b) the reference solution with 114 115 triangles.

TABLE 1

Global relative error err_{rel} for different values of thickness d and shape parameter ξ_0

	$\xi_0 = 0$	$\xi_0 = 0.25$	$\xi_0 = 0.5$
$d = 0.05$	0.072244	0.0726848	0.0724751
$d = 0.02$	0.0437599	0.0440597	0.0456497
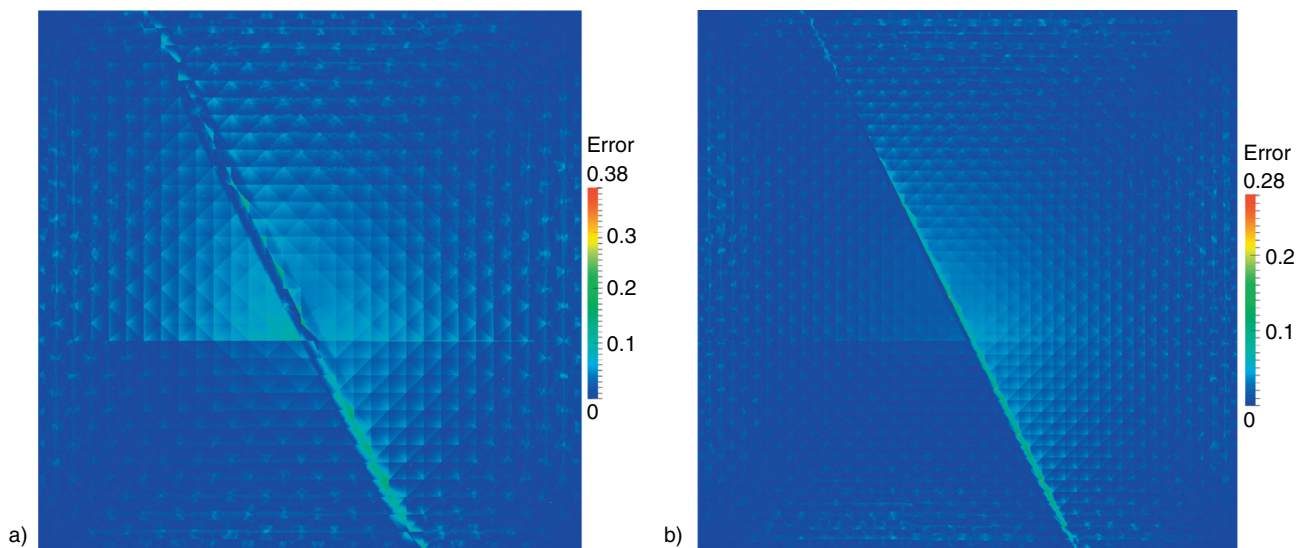
Figure 6

a) The model error (5) for thickness $d = 0.05$ while b) the model error (5) for thickness $d = 0.02$. In both simulation the shape parameter is $\xi_0 = 0.25$. In both figures the maximum error, 0.38 and 0.28 respectively, is obtained near the fracture in some very small elements.
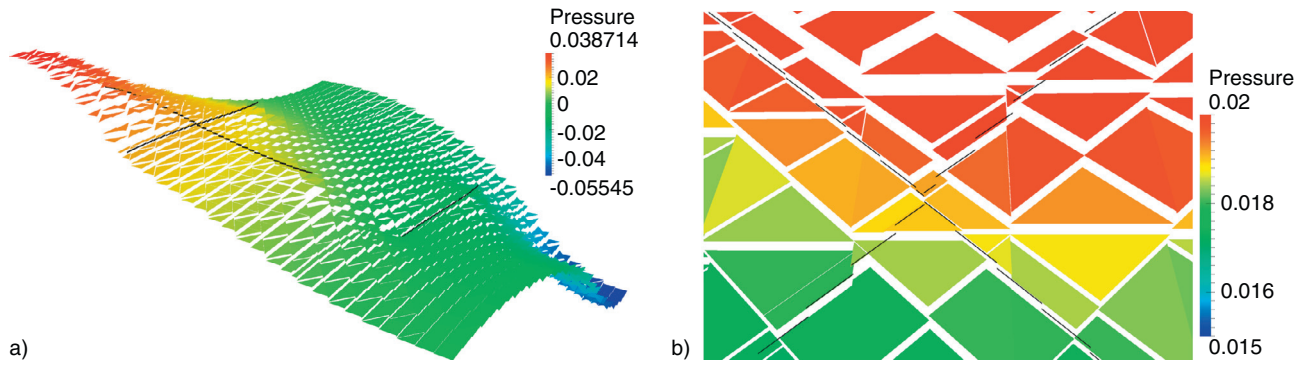
Figure 7

a) Pressure distribution for a "quarter of five spots" configuration in the presence of three intersecting and highly permeable fratures.
b) Zoom of the intersection showing the non conformity of the 2D and 1D grids.
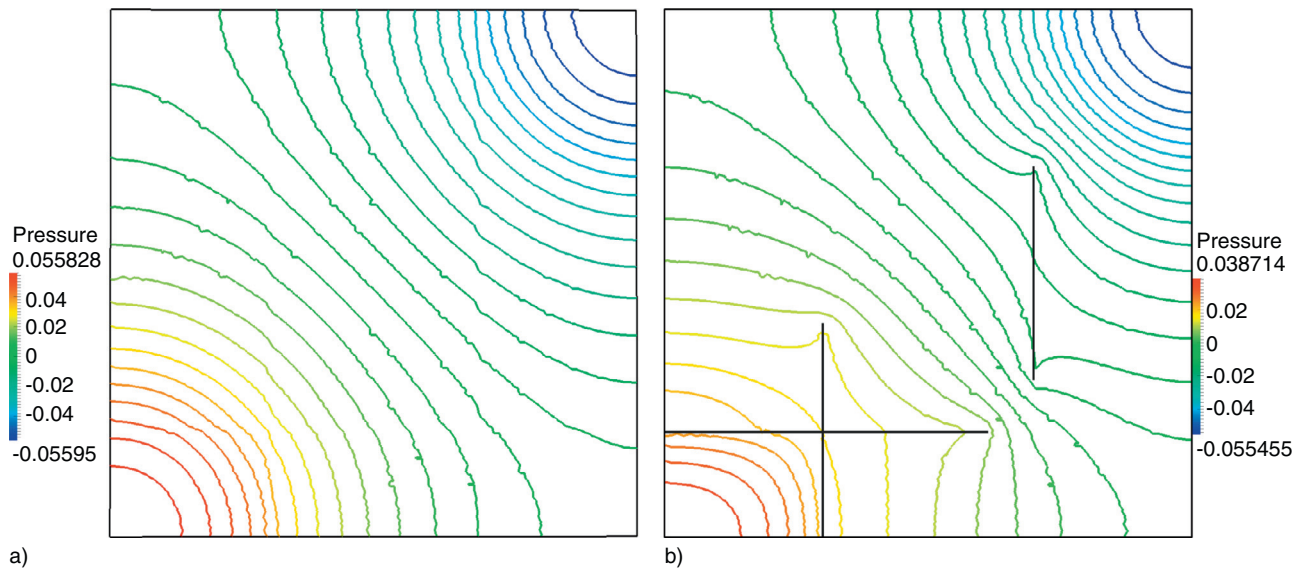
Figure 8

Plot of the pressure isolines in a) the absence and in b) the presence of three intersecting and highly permeable fractures.

of the same width $d = 0.01$ and permeability $K_{i,n} = K_{i,\tau} = 100$ for $i = 1, 2, 3$, while the permeability of the porous matrix is set to 1. The solution is reported in Figure 7, where the pressure distribution is obviously influenced by the presence of the fractures.

The zoom of the intersection region close to the injector shows that the fractures can cut the triangles of the mesh and, moreover, the grids of the fracture are independent on each other and also on the two-dimensional mesh. Figure 8 compares the isolines of pressure in the non fractured and fractured case, highlighting the effect of the higher conductivity due to the fractures.

CONCLUSIONS

In this paper, we have proposed a numerical method for the approximation of Darcy problems in fractured porous media. The main original aspect of this work, on the side of the mathematical modeling of subsurface flows, is to couple the reduced model for the flow in the fracture [6] with the flow across an intersection point [9]. Another important point is the increasing of the applicability of the proposed method, since we consider an approximation with the XFEM on two levels: in the matrix-fracture and in the fracture-fracture coupling.

We obtain a very flexible tool to solve these type of problems. In this work, we have assessed the validity of this approach comparing its results with those computed with the standard mixed finite element on a grid fine enough to resolve the fracture thickness. The solutions were in good agreement, except for the error introduced by the use of the reduced one-dimensional model for the fractures, that vanishes if the fracture aperture tends to zero. Moreover, the choice of the new coupling conditions, introduced in [9], for intersecting fractures allowed us to represent more general configurations such as the simultaneous presence of blocking and conductive fractures. Even if the method has been, so far, implemented only in the two-dimensional case where the fractures are represented as lines, it can already have an applicative interest, for instance, for the simulation of fractured reservoirs with numerical upscaling techniques. The development of the corresponding three dimensional method is the subject of ongoing and future works.

ACKNOWLEDGMENTS

REFERENCES

1 Alboin C., Jaffré J., Roberts J.E., Wang X., Serres C. (2000) *Domain decomposition for some transmission problems in flow in porous media, Lecture Notes in Phys.* **552**, 22-34, Springer, Berlin.

2 Martin V., Jaffré J., Roberts J.E. (2005) Modeling fractures and barriers as interfaces for flow in porous media, *SIAM J. Sci. Comput.* **26**, 5, 1667-1691, ISSN 1064-8275.

3 Angot P., Boyer F., Hubert F. (2009) Asymptotic and numerical modelling of flows in fractured porous media, *M2AN Math. Model. Numer. Anal.* **43**, 2, 239-275, ISSN 0764-583X.

4 Fumagalli A., Scotti A. (2011) Numerical modelling of multiphase subsurface flow in the presence of fractures, *Communications in Applied and Industrial Mathematics* **3**, 1, ISSN 2038-0909, doi: 10.1685/journal.caim.380.

5 Tunc X., Faille I., Gallouët T., Cacas M.-C., Havé P. (2012) A model for conductive faults with non-matching grids, *Computational Geosciences* **16**, 277-296, ISSN 1420-0597, doi:10.1007/s10596-011-9267-x.

6 D'Angelo C., Scotti A. (2012) A mixed finite element method for Darcy flow in fractured porous media with non-matching grids, *Mathematical Modelling and Numerical Analysis* **46**, 02, 465-489, doi: 10.1051/m2an/2011148.

7 Hansbo P. (2005) Nitsche's method for interface problems in computational mechanics, *GAMM-Mitt.* **28**, 2, 183-206, ISSN 0936-7195.

8 Amir L., Kern M., Martin V., Roberts J.E. (2005) Décomposition de domaine et préconditionnement pour un modèle 3D en milieu poreux fracturé, *Proceeding of JANO 8, 8th conference on Numerical Analysis and Optimization*, Dec.

9 Formaggia L., Fumagalli A., Scotti A., Ruffo P. (2013) A reduced model for Darcy's problem in networks of fractures, ESAIM: Mathematical Modelling and Numerical Analysis, in printing. DOI: 10.1051/m2an/2013132..

10 Hansbo A., Hansbo P. (2002) An unfitted finite element method, based on Nitsche's method, for elliptic interface problems, *Comput. Methods Appl. Mech. Engrg.* **191**, 47-48, 5537-5552, ISSN 0045-7825, doi: 10.1016/S0045-7825 (02)00524-8.

11 Hoteit H., Firoozabadi A. (2008) An efficient numerical model for incompressible two-phase flow in fractured media, *Advances in Water Resources* **31**, 6, 891-905, ISSN 0309-1708.

12 Karimi-Fard M., Durlofsky L.J., Aziz K. (2004) An Efficient Discrete-Fracture Model Applicable for General-Purpose Reservoir Simulators, *SPE Journal* **9**, 2, 227-236.

13 Brezzi F., Fortin M. (1991) Mixed and Hybrid Finite Element Methods, *Computational Mathematics* **15**, Springer Verlag, Berlin.